

Progress in CTEQ/TEA global QCD analysis

P. M. Nadolsky,^a J. Huston,^b H.-L. Lai,^c J. Pumplin,^b and C.-P. Yuan^b

^aDepartment of Physics, Southern Methodist University, Dallas, TX 75275, USA

^bDepartment of Physics & Astronomy, Michigan State University, E. Lansing, MI 48824, USA

^cTaipei Municipal University of Education, Taipei, Taiwan

We overview progress in the development of general-purpose CTEQ PDFs. The preprint is based on four talks presented by H.-L. Lai and P. Nadolsky at the 17th International Workshop on Deep Inelastic Scattering and Related Subjects (DIS 2009).

August 30, 2009

Interpretation of data from high-energy colliders, such as the Tevatron at Fermilab and the LHC at CERN, relies on the knowledge of parton distribution functions (PDFs) describing momentum distributions of quarks and gluons in the hadron. The most comprehensive method for determination of PDFs is based on a “global analysis” of many kinds of experiments, whose results are tied together by the theory of Quantum Chromodynamics (QCD). Historically, two families of general-purpose unpolarized PDFs have been in wide use, provided by the CTEQ [1] and MRST/MSTW [2] global analyses.¹ Members of CTEQ (Coordinated Theoretical-Experimental project on QCD) concurrently explore several kinds of PDFs [4, 5, 6]. Among these efforts, our group established and led for a long time by Wu-Ki Tung (which we will refer to as “Tung et al.”, or “TEA”, group) traditionally focuses on determination of general-purpose unpolarized proton PDFs and their uncertainties. The TEA group has presented four talks about its recent work at the DIS’2009 workshop in April 2009, with the slides available from the workshop website [7, 8, 9, 10]. The purpose of this contribution is to summarize those presentations. The main text will refer to the slides from the talks; it is essential to have them open when reading the paper.

CT09 set of parton distributions. In 2008, CTEQ/TEA group released a CTEQ6.6M best-fit PDF set [1], together with 44 supplementary PDF parametrizations needed for computation of PDF uncertainties. Our next set of PDFs to be released, tentatively designated “CT09”, will include a number of new features not available in CTEQ6.6. It will incorporate new experimental data that became recently available from the Tevatron Run-2 and address a number of physics issues impacting the behavior of the PDFs.

Tevatron jet production. The gluon distribution $g(x, \mu)$ remains among the least constrained parton distribution functions (PDFs), despite its important role in high-energy collider physics. Its behavior is most uncertain at momentum fractions x of order 0.1 or above, where the gluon PDF is constrained in the context of a global QCD analysis largely by the data on inclusive single-jet production at the Tevatron collider, $p\bar{p} \rightarrow \text{jet} + X$. Considerable freedom in the parametrization of $g(x, \mu)$ at large x values, still allowed by the global analysis, affects predictions for the Tevatron and LHC processes sensitive to gluon scattering, including production of high- p_T hadronic jets, $t\bar{t}$ pairs, and Higgs bosons.

Recently, the CDF and D0 collaborations at the Tevatron Run-2 published new measurements of inclusive single-jet production cross sections [11, 12, 13]. They have smaller

¹A third independent global analysis by Neural Network PDF Collaboration [3] is expected to be released in the near future.

statistical errors and better understood systematical uncertainties in comparison to similar Run-1 measurements [14, 15] available to CTEQ6.6. The impact of these Run-2 data on the gluon distribution were investigated as a part of the CT09 fit [16] and reviewed at the DIS'2009 workshop [7]. We focused, in particular, on the suggestion [2, 13] that the Run-2 data cause significant changes in the gluon PDF as compared to CTEQ6.6. If, for example, the Run-2 jet data prefer a smaller magnitude of $g(x, \mu)$ at large x , as suggested by the MSTW'2008 study, it would reverse the trend followed by the CTEQ5 and CTEQ6 PDF series that tended to have an enhanced gluon distribution in order to better accommodate the Run-1 jet cross sections.

In contrast to those suggestions, the CT09 analysis does not confirm that the Run-2 data necessitates suppression of $g(x, \mu)$ at large x . The main role of these data is to impose significant constraints on $g(x, \mu)$ and to reduce uncertainty in $g(x, \mu)$ at $x > 0.1$ despite relaxation of subjective assumptions about the gluon parametrization form made in the earlier global fits.

The CT09 best fit achieves excellent agreement with the Run-2 data [7, slides 5a, 5b], while also preserving tolerable agreement with the Run-1 data sets. The CT09 gluon PDF agrees with CTEQ6.6 within the uncertainty bands [7, slides 6 and 7]. The most significant difference between the CT09 and CTEQ6.6 $g(x, \mu)$ is observed at $\mu = Q < 5$ GeV and $x \approx 0.3$, where CT09 $g(x, \mu)$ is *enhanced* (rather than decreased) in comparison to CTEQ6.6 [7, slide 7, top left figure]. No significant differences between CT09 and CTEQ6.6 are observed at other x values or larger μ . This can be contrasted to the behavior of MSTW'08 NLO PDFs, also fitted to the Run-2 jet data and shown in the right figure of the same slide. While also enhanced above CTEQ6.6M at $x < 0.3$, the MSTW'08 NLO gluon PDF comes out to be systematically smaller than CTEQ6.6M at larger x . This discrepancy in the conclusions about the $x > 0.3$ region – suppression of MSTW'08 NLO $g(x, \mu)$ with respect to CTEQ6.6, and no discernible difference between CT09 and CTEQ6.6 – can be more a reflection of different choices made by the two groups (notably, in the selection of the functional form for $g(x, \mu)$) than of a genuine constraint by the Run-2 data (which become increasingly uncertain toward larger x).

Theoretical uncertainty. In light of the smallness of Run-2 statistical errors, uncertainty in $g(x, \mu)$ is now dominated by systematic factors, each of which needs to be explored in turn. To start, one must confirm that theoretical predictions for NLO jet production cross sections available from several groups [17, 18, 19, 20] agree within the desired accuracy of the analysis. We found [16] that differences between the EKS and FastNLO NLO calculations [17, 21] employed in the global analysis are smaller than, or comparable to, other systematic effects. At the same time, theoretical uncertainties due to factorization scales, hadronization, and underlying event can modify the jet cross sections by 10-20% [22]. Unimportant at present, this theoretical uncertainty will need to be accounted for in the future and eventually reduced by calculating jet cross sections at NNLO.

Agreement between single-jet production experiments; choice of PDF parametrization. The possibility of disagreement between the Run-1 and Run-2 inclusive jet data was repeatedly raised as an explanation for real or superficial differences between the pre- and post-Run-2 solutions for the gluon PDF. The best-fit gluon distribution obtained in a simultaneous fit to the the Run-1 and Run-2 jet data sets agrees with both; but, if fitted on their own, the Run-1 and Run-2 data prefer somewhat different shapes of $g(x, \mu)$. The degree of (dis)agreement depends on the functional form parametrizing $g(x, \mu_0)$ at the initial scale μ_0 . It can be exacerbated if the parametrization of $g(x, \mu)$ is insufficiently flexible.

To reduce the parametrization bias, CT09 employs a more flexible form for $g(x, \mu_0)$ than CTEQ6.6. This parametrization, designated as “par1” in [7, slide 15], includes five free parameters, vs. three parameters in CTEQ6.6. It leads to the best agreement with the experimental data sets — and it allowed us to systematically explore agreement between the jet experiments using a “ χ^2 reweighting method” proposed in [23] and a new “data set diagonalization” method described below.

This investigation shows that the Run-1 and Run-2 jet experiments are consistent, for the most part, with one another, with theory, and with non-jet experiments. Yet, peculiarities of presently unknown origin in the fit to the Run-1 data sets were also detected, which may explain their preference for a somewhat different gluon PDF. A persistently large $\chi^2/\text{d.o.f.}$ is observed in the case of the CDF Run-1 data regardless of the PDF parametrization used, reflecting excessive irregular scatter of these data. For the D0 Run-1 jet data, the χ^2 value varies excessively when very similar CTEQ parametrizations are compared. These effects may reflect underestimated uncorrelated errors present in the two measurements and, in the case of D0 Run-1, peculiar dependence on the cross section normalization and other correlated factors. Altogether, they may indicate insufficient control of systematic effects in Run-1 jet production.

In contrast to “par1”, less flexible gluon parametrizations tend to exaggerate tensions between the jet experiments, or between the jet and non-jet experiments. With such parametrizations, a good fit to all data sets required for the consistency study could not be attained. Consider, for example, a χ^2 reweighting scan exploring the agreement between the jet and non-jet data. The scan multiplies the jet data contribution χ_{jet}^2 to the global χ^2 by a weighting factor w_{jet} :

$$\chi^2 = w_{jet} \chi_{jet}^2 + \chi_{non-jet}^2.$$

Parametric dependence of χ_{jet}^2 and $\Delta\chi_{non-jet}^2 \equiv \chi_{non-jet}^2 - \min(\chi_{non-jet}^2)$ on w_{jet} is shown in the figure on slide 15 of [7]. The CT09 parametrization, “par1”, is compared to three-parameter (less flexible) parametrizations “par2” and “par3” defined on the same slide. Variations in χ^2 by 50-100 are deemed statistically significant in this comparison, in accordance with the CTEQ tolerance criterion [24]. Without the jet data included ($w_{jet} = 0$), the three parametrizations describe the non-jet data sets equally well ($\Delta\chi_{non-jet}^2 \approx 0$ for all three of them). When w_{jet} is increased to 1 (the jet and non-jet data are included on the same footing) or 10 (agreement with the jet data is strongly emphasized over the non-jet data), the “par1” form allows to significantly reduce χ_{jet}^2 , while only modestly increasing $\chi_{non-jet}^2$ ($\Delta\chi_{non-jet}^2 < 50$). This is less possible with the “par2” and “par3” forms: the reduction in χ_{jet}^2 happens only at the expense of a significant increase in $\chi_{non-jet}^2$, especially for “par3”.

HERA fits to DIS data commonly employ the “par3” form to parametrize the gluon distribution [25, 26, 27]. The total number of *all* free PDF parameters allowed in these fits cannot be larger than about 10 due to the limited constraining power of the DIS data fitted on its own. The χ^2 reweighting scan shows that the “par3” form is flexible enough to describe the DIS data on their own, but not to reconcile the DIS and Tevatron jet production constraints in a simultaneous global fit. In the latter case, a more flexible PDF parametrization such as “par1” can be introduced to provide a more realistic estimate of the PDF uncertainty.²

²In the NNPDF method [3], which operates with ultra-flexible PDF parametrizations, the primary effect of the jet data is to reduce the large uncertainty allowed for $g(x, \mu)$ by DIS experiments.

Data set diagonalization. The analysis of data sometimes requires fitting many free theoretical parameters to a large number of data points. Questions naturally arise about the compatibility of specific subsets of the data, such as those from a particular experiment or those based on a particular technique, with the rest of the data. Questions also arise about which theory parameters are determined by specific subsets of the data. In Ref. [28], an extension of the Hessian method for uncertainty analysis [29, 30] dubbed “data set diagonalization” (DSD) was developed in order to examine both kinds of questions.

The DSD procedure identifies the directions in the PDF parameter space along which a given subset \mathbf{S} of data provides significant constraints in a global fit. The procedure involves “a secondary diagonalization” of χ^2 to obtain a new set of fitting parameters $\{z_i\}$ that are linear combinations of the original ones. In the $\{z_i\}$ representation, the data set \mathbf{S} from a given experiment (or another subset of the full data) and its complement $\overline{\mathbf{S}}$ take the form of independent measurements, within the scope of the quadratic approximation applied to χ^2 . The degree of consistency between \mathbf{S} and $\overline{\mathbf{S}}$ can thus be examined straightforwardly by comparing two independent constraints on each parameter z_i considered.

When applied to practical fits [28], the DSD method uncovered and quantified the degree of tension between the two Tevatron Run-2 inclusive jet experiments, and between one of those experiments and the non-jet data, which was difficult to detect using the older χ^2 rescaling method. The DSD method can also identify which features of the fit are controlled by particular experiments or other subsets of the full data. As an example of this, the jet experiments were shown to be the principal source of information on the gluon distribution, by showing that the eigenvector directions dominating the uncertainty of the gluon distribution are the same directions that are constrained by the jet data (cf. Fig. 4 in [28]). More generally, the DSD method is suitable for a systematic study of consistency between experiments included in the full global fit (again within the scope of the Gaussian approximation) [31].

Correlation analysis of PDF uncertainties. In many practical applications, it may be necessary to know if the PDF uncertainty of one quantity, X , is related in any way to the PDF uncertainty of another quantity, Y . For example, one may need to establish if the PDF dependence of a specific cross section ($X = \sigma$) is driven by a specific PDF parameter ($Y = z_i$), constrained in turn by the measurement of another cross section, $Z = \sigma'$. These (often entangled) relations between the PDF dependence of different quantities can be elucidated by yet another technique extending the Hessian method, the PDF correlation analysis developed in Refs. [1, 30, 32]. The advantage of the correlation method as compared to the DSD or Lagrange multiplier methods is that publicly available error PDF sets are sufficient for carrying it out; it does not require specialized statistical tools.

In this approach [7, slides 22-24], one computes a cosine of correlation angle φ for X and Y ,

$$\cos \varphi = \frac{1}{4\Delta X \Delta Y} \sum_{i=1}^N \left(X_i^{(+)} - X_i^{(-)} \right) \left(Y_i^{(+)} - Y_i^{(-)} \right),$$

where $\Delta A = \sqrt{\sum_{i=1}^N \left(A_i^{(+)} - A_i^{(-)} \right)^2} / 2$ is the usual PDF error for $A = X$ or Y , and $A_i^{(\pm)}$ ($i = 1, \dots, N$) are the values of A evaluated for $2N = 44$ error PDF sets. One is most interested in situations when $\cos \varphi$ takes a value close to $+1$ or -1 . In these cases, the PDF dependence of X and Y is strongly correlated or anticorrelated, respectively, so that an accurate measurement of X would strongly reduce the PDF uncertainty of Y .

It is often instructive to calculate $\cos\varphi$ between a scattering cross section σ and a PDF $f_a(x, Q)$ at given x and Q . One can identify the PDFs and the x regions contributing the bulk of the PDF error to σ by plotting $\cos\varphi$ vs. x and looking for the x regions where $|\cos\varphi|$ is large (say, above 0.7). Figure 1 shows such plot for the total cross section of Z boson production at the LHC at $\sqrt{s} = 10$ TeV, while slide 24 in [7] shows the Z cross section at four chosen values of rapidity y of the Z boson. Each figure contains at least one curve with one or two x regions where $|\cos\varphi|$ is large. These x regions and PDF flavors drive the PDF uncertainty; the other regions are less important.

An interesting feature to notice is that the correlations for the total Z cross section are not reproduced exactly in either bin of the rapidity of the Z boson. The PDF uncertainty of the total cross section in Fig. 1 is correlated mostly with the least known c , b , and g PDFs at $x = 10^{-3} - 10^{-2} \sim M_Z/\sqrt{s}$, and not with the u , d quark and anti-quark PDFs that contribute the bulk of the cross section, but are constrained much better [1]. The Z cross section is also anti-correlated with the c , b , g PDFs at $x \sim 0.1$, as a consequence of the momentum sum rule. A similar correlation with the gluon and heavy-quark PDFs is observed at central rapidities ($y = 0.05$ and 1.05 in slide 24), however, these bins also show enhanced correlation with the strangeness distribution, which is not present in the total cross section. At large rapidity values of $y = 2.05$ $y = 3.85$, a strong correlation develops with the u and d (anti)quark PDFs, which overtakes the correlation with the gluon and heavy-quark distributions. As y increases, the position of the largest correlations shifts from $x = 10^{-2}$ at $y = 0.05$ to $x = 5 \cdot 10^{-4}$ at $y = 3.85$. The point of this exercise is to show that the PDF uncertainty of the total cross section is only an approximate predictor of the PDF dependence in the given process. More detailed studies may be needed when pronounced kinematical dependence of the PDF uncertainty is anticipated.

Intermediate-mass scheme for heavy quarks. A few-percent accuracy expected from the modern (N)NLO PDFs requires, among other things, to correctly implement heavy-quark mass contributions in cross sections in the whole energy range considered in the global analysis [1, 2, 33, 34]. This implementation is realized most systematically in the general-mass (GM) factorization scheme [35, 36], a recent implementation [33] of which is used in the CTEQ6.6 and CT09 fits. A good fraction of input precision data from DIS and fixed-target experiments included in the global analysis are at energy scales comparable to, or not too far above, the charm and bottom masses. The PDF parametrizations are thus sensitive to the more precise treatment of mass effects in the GM scheme. In turn, predictions for the Tevatron and LHC cross sections, including the benchmark W and Z cross sections, also depend on the treatment of heavy-quark masses at low energies.

Although the GM scheme is clearly superior in its consistency to the zero-mass (ZM)

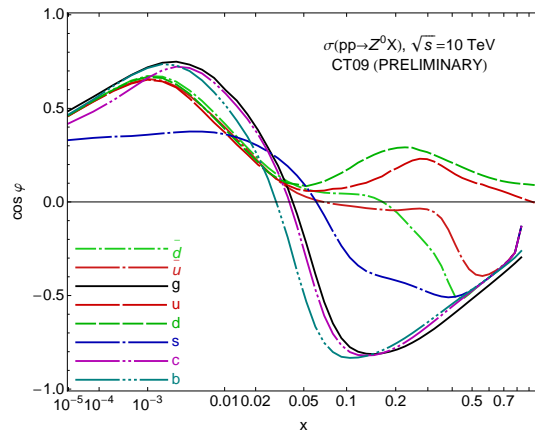


Figure 1: Correlation between the NLO total cross section for Z production at the LHC, $pp \rightarrow ZX$ at $\sqrt{s} = 10$ TeV, and PDFs $f_a(x, Q)$ at $Q = 85$ GeV.

scheme, it is considerably more complicated, and thus, not as widespread as the ZM scheme. On the other hand, since the most important heavy-quark mass effects reflect energy-momentum conservation in production of heavy quarks near their mass threshold, key features of the GM scheme might be potentially reproduced by implementing full mass dependence in the kinematical part of heavy-quark cross sections, while still assuming simplified zero-mass expressions for their dynamics described by the matrix elements [34]. This hybrid approach combining simple ZM dynamics with full GM kinematics was worked out in detail at NLO [8, 37]. The resulting effective formalism, which we proposed to call an “intermediate-mass (IM) calculational scheme”, can be viewed either as an improved zero-mass formulation with general-mass kinematics of final states, or a simplified general-mass formulation with zero-mass hard matrix elements. It can be applied to reproduce the essential heavy-quark mass dependence by a modest modification of the zero-mass calculation.

The exact implementation of the intermediate-mass approach is not unique, but depends on the choice of a rescaling variable ζ [8, slides 5-6]. For one specific choice of ζ (corresponding to the parameter $\lambda = 0.15$), all essential features of the general-mass scheme are reproduced both in terms of the resulting PDFs and in terms of typical physics predictions at the Tevatron and the LHC [8, slides 7-10]. These findings show that the IM scheme indeed brings the existing NLO analyses based on zero-mass hard matrix elements closer to the general-mass formulation. Nonetheless, dependence of the IM predictions on the form of the effective rescaling variable underlines the phenomenological nature of this approach. Although this dependence in principle also arises in the general-mass formalism, it is less pronounced than in the phenomenological IM formulation [8, slide 10]. Thus, the additional source of theoretical uncertainty due to the choice of the rescaling variable hardly affects what we know about the GM formalism – except that, perhaps, it should be added to the other sources of theoretical errors, such as scale dependence, when assessing the uncertainty of the GM theoretical results.

New data on vector boson production. The CT09 global analysis will include new data on heavy vector boson (W , Z) production produced in the Tevatron Run-2. This includes, first and foremost, the CDF measurements of charged lepton asymmetry in W boson production [38] and CDF Z boson rapidity distributions [39]. At this stage, we do not include the D0 Run-2 data on W boson charge asymmetry [40], since they cannot be well described by the global analysis. Agreement with these data can be only improved at the cost of having a much worse fit to the Run-1 W -lepton asymmetry data and non-Tevatron experiments. With the D0 Run-2 data in the fit, the ratio of down-valence to up-valence parton distribution functions in the large x region becomes too large as compared to the CTEQ6.6 uncertainty band. On the other hand, the W -lepton asymmetry data from CDF Run-2 agree well with the rest of the global analysis. CDF also released a new measurement of the W charge asymmetry as a function of W boson rapidity reconstructed from the 4-momentum of the charged lepton [41]. These data agree well with the recent CTEQ6.X PDFs, and its primary role would be to reduce the uncertainty in the relevant combinations of quark PDFs. For this, theoretical uncertainty arising in the reconstruction of the W boson rapidity distribution from the directly observed lepton distribution will need to be better understood.

Combined PDF + p_T fit. Recently, we extended the conventional global QCD analysis to include experimental data on transverse momentum (P_T) distributions in low- Q Drell-Yan and Z boson production in hadron-hadron scattering [9]. The P_T data is described systematically by Collins-Soper-Sterman resummation [42], which accounts for soft QCD radiation

that affects multi-scale measurements. Resummation introduces a phenomenological function $S_{NP}(b, Q)$ to describe nonperturbative QCD effects parametrized in impact parameter (b) space. Within the combined PDF+ P_T analysis, we are able to pursue determination of the nonperturbative function S_{NP} and the PDFs simultaneously. It is expected to give a better estimate for quantities that rely on both, especially for W boson mass measurement. As one of preliminary results, we obtained a new estimate of $S_{NP}(b, Q)$ at the invariant mass $Q = M_Z$ relevant for Z boson production in the Tevatron Run-2. By parametrizing $S_{NP}(b, M_Z) = gb^2$ and applying the Lagrange multiplier method, we found $g = 2.49^{+0.24}_{-0.39}$, which is slightly larger than the value of g reported by D0 collaboration [43]. We are in the process of producing a specialized set of error PDFs that will include additional PDF eigenvector sets to describe the uncertainty in $S_{NP}(b, Q)$.

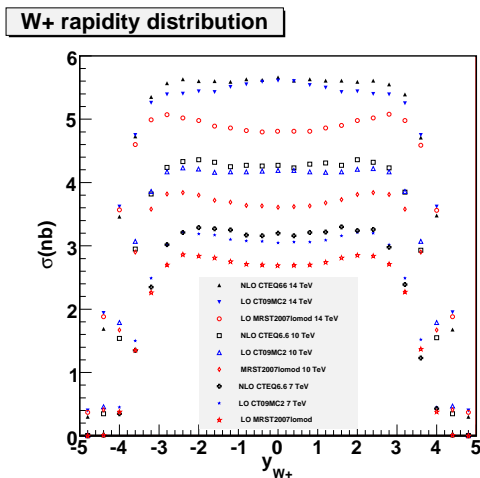


Figure 2: The $pp \rightarrow W^+ X$ cross section at $\sqrt{s} = 10$ and 14 TeV, from the NLO/CTEQ6.6 calculation and LO calculations based on CTEQ and MSTW modified LO PDFs.

global fit along with the usual experimental data. Specific pseudodata sets considered were for W , Z , $t\bar{t}$, $b\bar{b}$, and Standard Model Higgs boson production in pp collisions at 14 TeV, generated at NLO using the CTEQ6.6 set of PDFs. The purpose of the pseudodata is to enhance the desired NLO behavior in the LO MC PDFs. Two approaches were adopted: (1) the momentum sum rule was kept intact, and the scales for the pseudodata cross sections were varied within a limited range to achieve the best fit to the shape of the relevant NLO kinematic distributions; or (2) violations of the momentum sum rule were allowed, and the best LO fit to the pseudodata cross sections was attempted, in terms of both normalization and shape. An example of the latter approach is shown in Figure 2, where the W^+ rapidity distribution at the LHC is shown for center-of-mass energies of 14, 10 and 7 TeV. The CTEQ LO MC PDF (CT09MC2) leads to better agreement with the fully NLO prediction at 14 TeV than the LO prediction using the MRST2007lomod PDF, both in the shape of the W^+ rapidity distribution and in its normalization. Good agreement is also observed for the predictions for the two lower center-of-mass energies for the LHC. A similar level of agree-

PDFs for leading order Monte-Carlo showering programs.

Just as NLO PDFs are used with NLO calculations, it has been natural to use LO PDFs with LO calculations, including the popular parton shower Monte Carlo programs. Unfortunately, many collider matrix element calculations realized at LO differ from NLO predictions not only in magnitude, but also in shape, because of the impact of hard-scattering corrections, but also because of the differences existing between the LO and NLO PDFs. This problem has led to the introduction of PDFs that are specially designed for leading-order Monte Carlo (LO MC) programs. They attempt to lessen the differences between the LO and NLO predictions by modifying the PDFs. Such LO MC PDFs have been produced recently by CTEQ/TEA [10]. In our approach, pseudodata for NLO *theoretical* cross sections for several benchmark collider processes have been included in the

ment is achieved for the W^- and Z cross sections, and better shapes and normalizations are obtained for the heavy-flavor and Higgs cross sections as well.

PDF reweighting and FROOT. In a typical calculation of the PDF uncertainty, the user must compute the cross section of interest for a large number ($N = 30 - 1000$) of error PDFs. A multi-loop QCD calculation for *even one PDF set* can require substantial computer resources. Straightforward repetition of this calculation for *many PDF sets* can quickly become intractable.

This bottleneck can be eliminated by a general-purpose technique for event reweighting in Monte-Carlo integration programs. The event reweighting reduces the CPU time needed to compute all N cross sections by evaluating complicated multi-loop matrix elements only once for all N PDFs. The event reweighting also improves convergence of the Monte-Carlo estimate for the PDF uncertainty [7, slides 25-26].

The TEA group develops FROOT [44], a publicly available library that facilitates PDF reweighting and analysis of large numerical outputs for many PDF sets in theoretical calculations written in Fortran or C++. The current version of FROOT provides a simple interface to write differential cross sections for N PDF sets into CERN ROOT trees, which can then be analyzed inside the ROOT program to evaluate PDF uncertainties, PDF correlations, etc. Depending on the setup of the calculation, this approach can substantially reduce (by a factor of 10 or more) the requirements for CPU time and hard-disk storage requirements. The FROOT interface is implemented in MCFM [45, 46, 47] and ResBos programs [48, 49] computing a variety of theoretical cross sections. In the future, FROOT will be expanded to include additional features facilitating the analysis of the PDF dependence of collider cross sections in CERN ROOT.

Acknowledgments

This research was supported by the U.S. Department of Energy under grant DE-FG02-04ER41299; U.S. National Science Foundation under grants PHY-0354838, PHY-055545, and PHY-0757758; National Center for Theoretical Sciences and National Science Council of Taiwan grant NSC-97-2112-M-133-001; by LHC Theory Initiative Travel Fellowship awarded by the U.S. National Science Foundation under grant PHY-0705862; and by Lightner-Sams Foundation.

References

- [1] P. M. Nadolsky *et. al.*, Phys. Rev. **D78**, 013004 (2008).
- [2] A. D. Martin, W. J. Stirling, R. S. Thorne, and G. Watt, Eur. Phys. J. **C63**, 189 (2009).
- [3] NNPDF Collaboration, R. D. Ball *et. al.*, Nucl. Phys. **B809**, 1 (2009).
- [4] C. Keppel, <http://indico.cern.ch/contributionDisplay.py?contribId=98&confId=53294>.
- [5] I. Schienbein *et. al.*, [arXiv:0907.2357](https://arxiv.org/abs/0907.2357).
- [6] D. de Florian, R. Sassot, M. Stratmann, and W. Vogelsang, Phys. Rev. **D80**, 034030 (2009).

- [7] P. Nadolsky, <http://indico.cern.ch/contributionDisplay.py?contribId=88&confId=53294>.
- [8] P. Nadolsky, <http://indico.cern.ch/contributionDisplay.py?contribId=173&confId=53294>.
- [9] H.-L. Lai, <http://indico.cern.ch/contributionDisplay.py?contribId=89&confId=53294>.
- [10] H.-L. Lai, <http://indico.cern.ch/contributionDisplay.py?contribId=313&confId=53294>.
- [11] CDF Collaboration, T. Aaltonen *et. al.*, Phys. Rev. **D78**, 052006 (2008).
- [12] CDF Collaboration, A. Abulencia *et. al.*, Phys. Rev. **D75**, 092006 (2007).
Erratum: *ibid.*, **D75**, 119901 (2007).
- [13] D0 Collaboration, V. M. Abazov *et. al.*, Phys. Rev. Lett. **101**, 062001 (2008).
- [14] CDF Collaboration, A. A. Affolder *et. al.*, Phys. Rev. **D64**, 032001 (2001).
Erratum: *ibid.*, **D65**, 039903 (2002).
- [15] D0 Collaboration, B. Abbott *et. al.*, Phys. Rev. **D64**, 032003 (2001).
- [16] J. Pumplin, J. Huston, H. L. Lai, P. M. Nadolsky, W.-K. Tung, and C.-P. Yuan,
Phys. Rev. **D80**, 014019 (2009).
- [17] S. D. Ellis, Z. Kunszt, and D. E. Soper, Phys. Rev. Lett. **69**, 1496 (1992).
- [18] W. T. Giele, E. W. N. Glover, and D. A. Kosower, Nucl. Phys. **B403**, 633 (1993).
- [19] Z. Nagy, Phys. Rev. Lett. **88**, 122003 (2002).
- [20] Z. Nagy, Phys. Rev. **D68**, 094002 (2003).
- [21] T. Kluge, K. Rabbertz, and M. Wobisch, [hep-ph/0609285](http://arxiv.org/abs/hep-ph/0609285).
- [22] F. I. Olness and D. E. Soper, [arXiv:0907.5052](http://arxiv.org/abs/0907.5052).
- [23] J. C. Collins and J. Pumplin, [hep-ph/0105207](http://arxiv.org/abs/hep-ph/0105207).
- [24] J. Pumplin *et. al.*, JHEP **07**, 012 (2002).
- [25] ZEUS Collaboration, S. Chekanov *et. al.*, Eur. Phys. J. **C42**, 1 (2005).
- [26] H1 Collaboration, [arXiv:0904.3513](http://arxiv.org/abs/0904.3513).
- [27] V. A. Radescu, AIP Conf. Proc. **1105**, 114 (2009).
- [28] J. Pumplin, [arXiv:0904.2425](http://arxiv.org/abs/0904.2425).
- [29] J. Pumplin, D. R. Stump, and W. K. Tung, Phys. Rev. **D65**, 014011 (2001).
- [30] J. Pumplin *et. al.*, Phys. Rev. **D65**, 014013 (2001).
- [31] J. Pumplin, [arXiv:0909.0268](http://arxiv.org/abs/0909.0268).
- [32] P. M. Nadolsky and Z. Sullivan, [hep-ph/0110378](http://arxiv.org/abs/hep-ph/0110378).
- [33] W. K. Tung *et. al.*, JHEP **02**, 053 (2007).
- [34] R. S. Thorne and W. K. Tung, [arXiv:0809.0714](http://arxiv.org/abs/0809.0714).

- [35] J. C. Collins, Phys. Rev. **D58**, 094002 (1998).
- [36] M. A. G. Aivazis, J. C. Collins, F. I. Olness, and W.-K. Tung, Phys. Rev. **D50**, 3102 (1994).
- [37] P. M. Nadolsky and W.-K. Tung, Phys. Rev. **D79**, 113014 (2009).
- [38] CDF Collaboration, D. E. Acosta *et. al.*, Phys. Rev. **D71**, 051104 (2005).
- [39] CDF Collaboration, T. Aaltonen *et. al.*, [arXiv:0908.3914](https://arxiv.org/abs/0908.3914).
- [40] D0 Collaboration, V. M. Abazov *et. al.*, Phys. Rev. Lett. **101**, 211801 (2008).
- [41] CDF Collaboration, T. Aaltonen *et. al.*, Phys. Rev. Lett. **102**, 181801 (2009).
- [42] J. C. Collins, D. E. Soper, and G. Sterman, Nucl. Phys. **B250**, 199 (1985).
- [43] D0 Collaboration, V. M. Abazov *et. al.*, Phys. Rev. Lett. **100**, 102002 (2008).
- [44] The source code for FROOT, version 1.0 can be downloaded at <http://hep.pa.msu.edu/cteq/public/froot/froot1.0.tar.gz> .
- [45] J. M. Campbell and R. K. Ellis, Phys. Rev. **D62**, 114012 (2000).
- [46] J. Campbell, R. K. Ellis, and F. Tramontano, Phys. Rev. **D70**, 094012 (2004).
- [47] J. Campbell and F. Tramontano, Nucl. Phys. **B726**, 109 (2005).
- [48] C. Balazs and C.-P. Yuan, Phys. Rev. **D56**, 5558 (1997).
- [49] F. Landry, R. Brock, P. M. Nadolsky, and C.-P. Yuan, Phys. Rev. **D67**, 073016 (2003).